Supporting Information for

The unlocking process leading to the 2016 Central Italy seismic sequence

Sugan M.[1], Campanella S.[1], Chiaraluce L.[2,1], Michele M.[2], Vuan A.[1,2]

[1] National Institute of Oceanography and Applied Geophysics – OGS (Italy)

[2] Istituto Nazionale di Geofisica e Vulcanologia (Italy)

Contents of this file:

TEXT S1 - ***Input catalog***

All the events initially recorded and located by the Italian National Network and Seismological Data Centre (INGV Seismological Data Centre 2006; ISIDe Working Group, 2007) have been relocated in absolute terms using NonLinLoc code (Lomax et al., 2000), based on a nonlinear inversion method (Figure S1 in the supplement). We used the same 1D gradient velocity model and setup used by Chiaraluce et al. (2017); we also included station corrections to counteract the effects of using an oversimplified velocity model. These preliminary locations already have good quality factors, as shown in Michele et al. (2019), with most events (~66%) included in the A and B quality classes (see Figure S2 in the supplementary material).

To further maximize the quality of the templates' catalog in terms of hypocentral location resolution, we apply a double difference (Waldhauser and Ellsworth, 2000) scheme taking only absolute travel times. In the relative relocation process, we used the same setup proposed by Michele et al. (2020) for relocating the 2016 aftershocks sequence. We kept all the M_L>1.5 events of the 2016 sequence together with the previous events to be relocated. In doing this, we additionally constrain the depth of the whole system (see Figure S3). We selected a well-constrained subset of events to obtain more robust quantitative estimates of coordinates location errors of the final catalog we used as input for the template matching. We relocated them using the full covariance matrix and singular value decomposition (SVD) instead of the weighted least squares (LSQR) method (see Waldhauser and Ellsworth, 2001).

TEXT S2 - ***Template matching***

Template matching is run to search about eight years (2009-2016) of continuous data exploiting approximately 23,000 well-located earthquakes in Central Italy. Codes are rewritten from Vuan et al. (2018) to improve performance and scalability, evaluate background seismicity, and analyze clustering before the 2016 sequence in Central Italy.

The technical improvements needed to address massive computations involved: a) performance: ≈200% speedup in single-threaded mode, near-linear scaling using multiple threads. GPU support with further performance improvements: 50 templates per second per node with 4 GPU (NVIDIA V100), and higher speedups possible

using longer signals. Faster post-processing thanks to AVRO/Parquet data serialization, b) usability: CLI, logging, input and output handling, arbitrary signal length, template duration (per channel basis), and sampling rate, c) robustness & correctness: better error handling, among fixed bugs: negative normalization in Obspy cross-correlation routine, drop multiple detections within template length, more stable magnitude estimation (missing data, template data and other bug fixes), detections at beginning or end of the signal, full usage of data (template/signal traces matching before processing), d) maintainability: less code (-80%) and dependencies, enhanced readability (refactoring into functions, meaningful variable nomenclature), modularity, easier deployment via registered PyPI package.

Template matching is applied to daily three-component continuous waveforms covering the 2009/01/01-2016/08/24 time window. Seismic data from 2009 to 2016 are collected for 37 stations of the INGV seismic network (STATION_LIST in the supplement).

The performance of the seismic network necessarily varies when a long period is considered. Figure S4 shows the channel's daily data availability over time. From 2009, at least 40 channels were available, while the seismic network became pretty stable in 2012, with a minimum of 70 channels always available.

We also investigate the existence of data gaps (hours) that, on average, amount to 1.5% of the available dataset, with a minimum and maximum of about 0.16% and 4.6%, respectively.

We resample waveform data to 20 Hz and apply a 3-8 Hz bandpass filter. The adopted frequency band is appropriate considering the seismic network configuration, the events' size, the studied region's extent, and the analyzed period. A similar setting was used for the template matching analysis of the Amatrice, Aquila, and Alto Tiberina regions (Vuan et al., 2017; 2018; 2020).

A higher frequency band, suitable for detecting events of smaller magnitude, was used in some studies to analyze events near faults, using closer stations, sometimes even borehole stations, characterized by a high signal-to-noise ratio (e.g., Cabrera et al., 2020).

Templates are trimmed using a 5 s data window, starting 2.5 s before the theoretical S wave arrival, computed using the ObsPy port (Krischer et al., 2015) of the Java TauP Toolkit routines (Crotwell et al., 1999) and a suitable 1D-model (a modified version of Carannante et al., 2013).

Based on the seismic network configuration and magnitude ranges, we fixed an event to station distance cutoff at 60 km, avoiding using the farthest channels. Moreover, we adopt a Kurtosis-based test to evaluate the signal-to-noise ratio of templates (Baillard et al., 2014), excluding noisy signals in the template matching technique (Vuan et al., 2018; Vuan et al., 2020). We fix the maximum number of channels up to 18 to speed up computation. This approach guarantees a good input data quality for the template matching procedure. A match, or candidate detection, is a peak above a given threshold, set to 0.4, in the average of the stacked correlograms. The threshold was defined after visual inspection of 500-subset data to avoid false detections. Lower cross-correlation values provide noisy detections especially observed during the data gaps.

The fluctuating performance of the seismic network means that two ideals in a seismic catalog conflict because we want to detect as many events as possible and provide a consistent detection threshold over time. In creating the extended catalog, we chose a compromise and tried to maintain a roughly constant detection threshold before and after 2012. In particular, in the post-processing phase, detections have been dropped based on the ratio between the average cross-correlation and the noise baseline level, estimated via the daily Median Absolute Deviation (MAD) of the correlograms. Keeping only the detections with a high ratio proved a robust method to exclude artifacts and false detections. The threshold for this ratio, defined after a visual inspection of some examples of detected events, was set to 18 times the MAD. Figure S5 in the supplementary material shows an example of a single detection associated with a specific template and the seismic waveforms associated with different detections for the same template at the closest station.

Time windows of 6 s are selected. Within each one, the template for which the normalized correlation coefficient is the greatest is taken to determine the event location and magnitude (e.g., Kato et al., 2012). In synthesis, in declaring a detection, we use very restrictive criteria: a) the average cross-correlation must be greater or equal to 0.4, b) it must be also greater or equal to 18 times the MAD, and c) at least 8 channels must have cross-correlation greater or equal to 0.4.

The location of the small events in the augmented catalog strictly depends on the quality of the input catalog locations and associated errors. Due to the high resolution of the starting catalog, we decided to keep the new detections co-located with the templates.

This choice of not relocating the new events is partly justified by the area dimensions (100 x 100 km), the seismic station's inter-distance relative to the area under study, and the reduced number of earthquakes for which it is possible to obtain a more refined location. Ross et al. (2019) and Simon et al. (2021), demonstrated that only a small portion of events from template matching could be relocated (on average less than 20%). Moreover, relocation techniques based on limited frequency-band envelopes (e.g., Vuan et al., 2017) cannot improve the location of small magnitude events when the network coverage is sparse. These considerations led us to co-locate the new events at the respective template position.

The magnitude is estimated by amplitude comparison with the templates. A tenfold increase in the amplitude ratio corresponds to a one-unit increase in magnitude at each recording channel (Peng and Zhao 2009).

To improve the robustness of the magnitude assessment, we removed the outliers in the pool of used channels (e.g., Ross et al., 2019).

TEXT S3 - *Clustering*

A nearest-neighbor approach (Zaliapin and Ben-Zion, 2016) performs a statistical analysis of the augmented catalog to separate the background seismicity from the clusters. The nearest-neighbor method computes the time-space distance η between pairs of earthquakes. Rescaled time (T) and distance (R) between an event *i* and its parent *j* are normalized by the magnitude of *j* and expressed as:

$$T_{ij}=t_{ij}10^{-pbm_i/2};\ R_{ij}=r_{ij}^{d}10^{-(1-p)bm_i/2} \quad (1)$$

Where *p* is a weight parameter, *b* is the Gutenberg-Richter value, *m is* the magnitude of the *i* event, *t* and *r* are the time and distance between the two earthquakes, respectively, and *d* is the fractal dimension. We fixed *p*=0.5, *b*=0 (Zaliapin and Ben-Zion (2020) justify using *b*=0 for small events) and *d*=1.6. Thus, η, the generalized distance between pairs of earthquakes, is formulated as:

$$\text{Log } \eta_{ij}=\log R_{ij}+\log T_{ij} \quad (2)$$

Eq. (1) requires the distance between events (rij), which in the case of co-located events (template and its detections) is 0 leading to Rij=0.

Using the distribution of interevent times for spatially close events, we tried to check if some multi-modality could suggest how to separate the related events from the independent ones.

Results from this analysis, performed for some clusters, evidenced that the problem does not affect our results. However, we noticed that some events could be included in the same cluster, even if the cluster activity is off for some time and reactivates later. To overcome the problem, we sorted clusters in sub-clusters at similar positions using a cutoff time window when no events were found for a week.

Figure S6 in the supplementary shows the generalized earthquake distance η (eq. 2) and density obtained for the augmented catalog, giving the classification quality between background and clustered seismicity.

Subsequently, clusters with at least 10 events are classified into swarms, mainshock-aftershock, and foreshock-mainshock sequences following the criterion proposed by Ogata and Katsura (2012). Figure S7 in the supplement shows an example of the classification applied. The mainshock is the strongest earthquake in a cluster, and all the previous seismic events are pre-shocks. All pre-shocks are set foreshocks when the magnitude gap between the largest pre-shock and the mainshock is greater than 0.5. Unlike, a swarm-like sequence has pre-shocks with similar magnitudes (the difference is smaller than 0.5).

Further indications on clustering are also provided by comparing the coefficient of variation with the moment ratio variations. The coefficient of variation of interevent times (e.g., Kagan and Jackson, 1991) defines temporal clustering as close to 0 for periodic seismicity and greater than 1 for temporally clustered sequences. The seismic moment ratio values (Cabrera et al., 2022), defined as the ratio of the maximum seismic moment to the total seismic moment of the analyzed window, provide indications when most of the seismic moment can be associated with a single event (values close to 1) or when no prevailing event is found (values relative to 0).

The coefficient of variation and moment ratio are evaluated using rolling windows of a variable number of events (50 to 150 with a step of 10). We also derive the associated uncertainties by averaging the results of the different rolling windows. In Figures 4, S15 and S16 (the last two in the supplement), we represented the resulting mean plus/minus one standard deviation.

TEXT S4 - ***Repeating earthquakes***

We search for repeating earthquakes, families of two or more events with nearly identical waveforms, locations, geometry, and magnitudes that repeatedly rupture the same fault patch at different times (e.g., Uchida 2019). We analyze the overall cross-correlation output of the template matching procedure, looking for couples of events characterized by a mean cross-correlation value >=0.90. Then we group events sharing common events and compile a list of candidate repeating earthquakes (CRE). Events span in magnitude range from about 0.4 to 2.6.

This dataset is further investigated using a Python code for detecting true repeating earthquakes from self-similar waveforms. The code combines seismic waveform similarity using cross-correlation (CC) and differential S-P travel times (Sugan et al., 2022). Precise differential ΔS–P arrival times between CRE pairs are obtained by applying the cross-spectral method described in Poupinet et al. (1984). The spectral method is preferred since it allows sub-sample precision to resolve minimal source separation. We use 0.97 CC value and different ΔS−P thresholds indicating possible RE that share at least 50% of the seismic source.

Between these thresholds, the similarity space domain (SSD) took place, and the number of seismic stations inside it can be evaluated for proper RE identification (Chen et al., 2008). r is estimated using the following equation (e.g., Eshelby 1957):

$r = ((7/16)(M_o/\Delta\sigma))^{1/3}$ (1),

where M_o is the seismic moment, and Δσ is the uniform stress drop. We use the ML-Mw conversion following Munafò et al. (2016) to calculate M_o and assume 3MPa Δσ. ΔS−P thresholds (Table 1) are obtained based on the seismic source radius and velocity model used for the template matching procedure.

The code needs as input a CRE catalog, the associated seismic waveforms, the associated P and S picks, if any, and a simple 1D velocity model.

We use the original seismic waveforms sampled at 100Hz, and the travel-time phase file to localize the templates. When this information is missed (e.g., for the new detections obtained with template matching), we use the theoretical arrival times calculated using a suitable velocity model (Carannante et al., 2013) or perform automatic picking using STA/LTA strategies.

We explore different frequency configurations, considering up to four magnitude ranges. We set a minimum of three stations in the similarity space domain to declare a RE (Table 1). Cross-correlation values are calculated for a time window starting 0.5

seconds before the P arrival phase and ending 12 seconds after the S phases. Cross-spectrum is evaluated for P and S wave time windows with a length of about 1.4 s and 1.8 s, respectively.

We found a maximum number of 16 RE for configuration #1 and a minimum number of 6 RE for configuration #3. They are doublets, characterized by short interevent times (less than 17 hours); only one RE exceeds this value, with an inter event time of about 23 days (RE events occurred on 18 May and 10 June 2009).

In Table 2 we show the information about one of the most constrained configurations, the Conf#2 RE pairs: origin times, magnitudes, intervent times, and estimated source size. Most of these RE occur at depth > 7 km, below the TSZ, or the transition zone between the shallow seismicity and the SZ.

Figure S8 shows the location on the map and time distance along the strike of the overall seismicity and RE for the configurations shown in Table 1. The final RE's position for each doublet is obtained using the mean value of the events' latitude and longitude.

		Conf#1	Conf#2	Conf#3
	SSD	***CC 0.97***		
ML	***ΔS–P (sec)***	BP(Hz)	BP(Hz)	BP(Hz)
0.5 ≤ ML < 1	***0.004***	1-30	1-35	1-40
1≤ ML < 1.5	***0.006***	1-25	1-30	1-35
1.5 ≤ ML < 2	***0.009***	1-20	1-25	1-30
ML ≥ 2	***0.01***	1-15	1-20	1-25
	RE	16	7	6

Table 1

ΔS–P and CC values for #3 different configurations used to define the similarity space domain (SSD). Variable band-pass filters (BP) for different magnitudes (ML) ranges are explored. For each configuration, the corresponding number of RE is shown.

RE pair id	Origin time (F**, S**, M*, A*)	Magnitude (Depth[km])	Interevent times (sec)	Source size (m)
1	2014-06-12T02:13:58.994(M)* 2014-06-12T05:34:03.177(F)**	1.4 (7.17) 1.5 (7.50)	12005	62.5 67.5
2	2014-06-26T15:10:52.394(F)** 2014-06-26T16:55:24.979(F)**	1.2 (10.6) 1.1 (10.7)	6272	53.6 49.7
3	2015-05-19T05:31:25.255(M)* 2015-05-19T06:28:09.121(M)*	1.5 (8.35) 1.7 (8.4)	3404	67.5 78.7
4	2009-05-18T17:19:41.280(S)** 2009-06-10T22:21:06.560(S)**	2.2 (8.51) 2.2 (8.50)	2005285	115.6 115.6
5	2011-11-07T02:29:26.150(F)** 2011-11-07T02:22:23.466(F)**	1.6 (11.1) 0.9 (11.0)	423	72.9 42.6
6	2012-12-20T21:00:16.530(S)** 2012-12-20T19:45:50.028(S)**	1.6 (8.67) 1.6 (8.67)	4466	72.9 72.9
7	2015-03-27T22:56:54.954(A)* 2015-03-27T20:44:57.593(A)*	1.3 (3.93) 1.2 (3.93)	7917	57.9 53.6

Table 2

RE pairs, Conf#2 in Table 1: identification number (RE pair id), origin time, classification (F**=Foreshock-mainshock, S**=Swarm, M*=Mainshock, A*=Aftershock), magnitude and depth (original catalog), interevent time, and estimated source size.

*classification based on Zaliapin and Ben-Zion (2016) for background seismicity and clusters with less than 10 events;

**classification based on Zaliapin and Ben-Zion (2016) and Ogata and Katsura (2012) for clusters with at least 10 events.

MS1 and MS2 Movies description

Two movies (MS1 and MS2) show where seismicity is localized and how it evolves above and below the shear zone top (TSZ). MS1 indicates a migration of shallow seismicity within the main fault volume while MS2 shows an increasing seismicity rate at the two main fault edges at depth below the supposed sub-horizontal shear zone. These observations also suggest that deformation is progressive and localized at the two tips at depth favoring an unlocking of the normal fault.

MS3 Movie description

The MS3 3D movie shows the temporal evolution of the pre-sequence seismicity and the location of the fault planes activated during the 2016 seismic sequence - Amatrice (red, Tinti et al., 2016), Visso (orange, Chiaraluce et al., 2017) and Norcia (blue, Scognamiglio et al., 2018). The seismicity is mainly located at depth in the southern and northern sectors, at the edges and in the hanging wall of the fault planes.

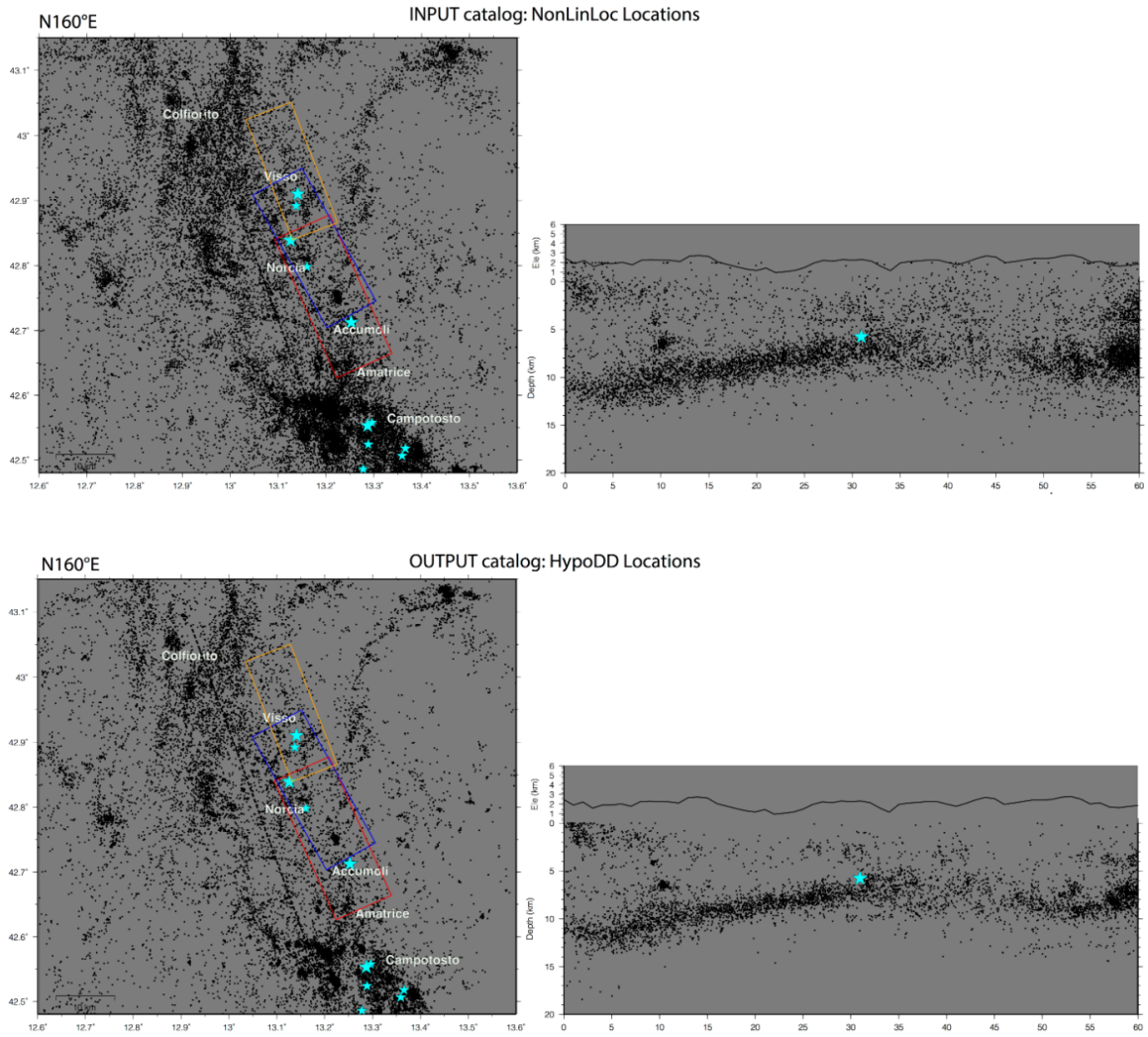

Figure S1

Map-view (left) and related cross-sections (right), reporting the earthquakes location of the input catalog (NonLinLoc absolute locations), on the top, compared to the output catalog (HypoDD relative locations) on the bottom. Map-views show the faults projected for the Amatrice mainshock (red line), Visso (orange line), and Norcia (blue line); dashed black lines represent the traces referring to the cross-sections on the right. These are oriented along the main strike and seismicity in a 15 km wide area around the traces. In all the figures, cyan stars mark the position of the Mw >= 5.0 mainshocks.

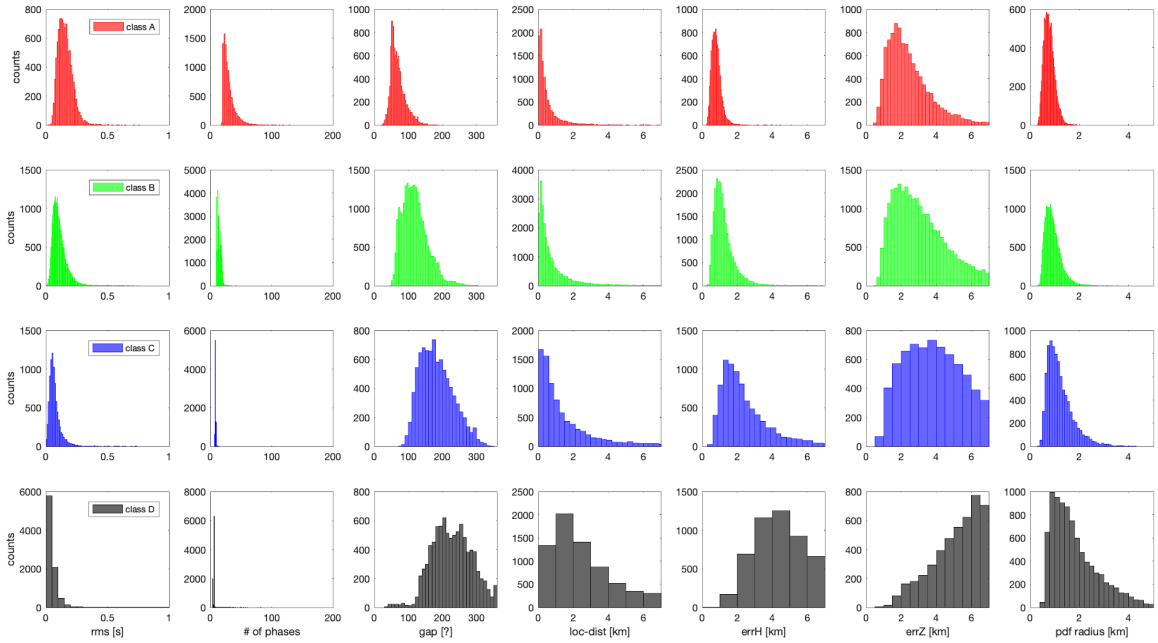

Figure S2

Statistical distribution of the uncertainty estimators used to evaluate the location quality factor.

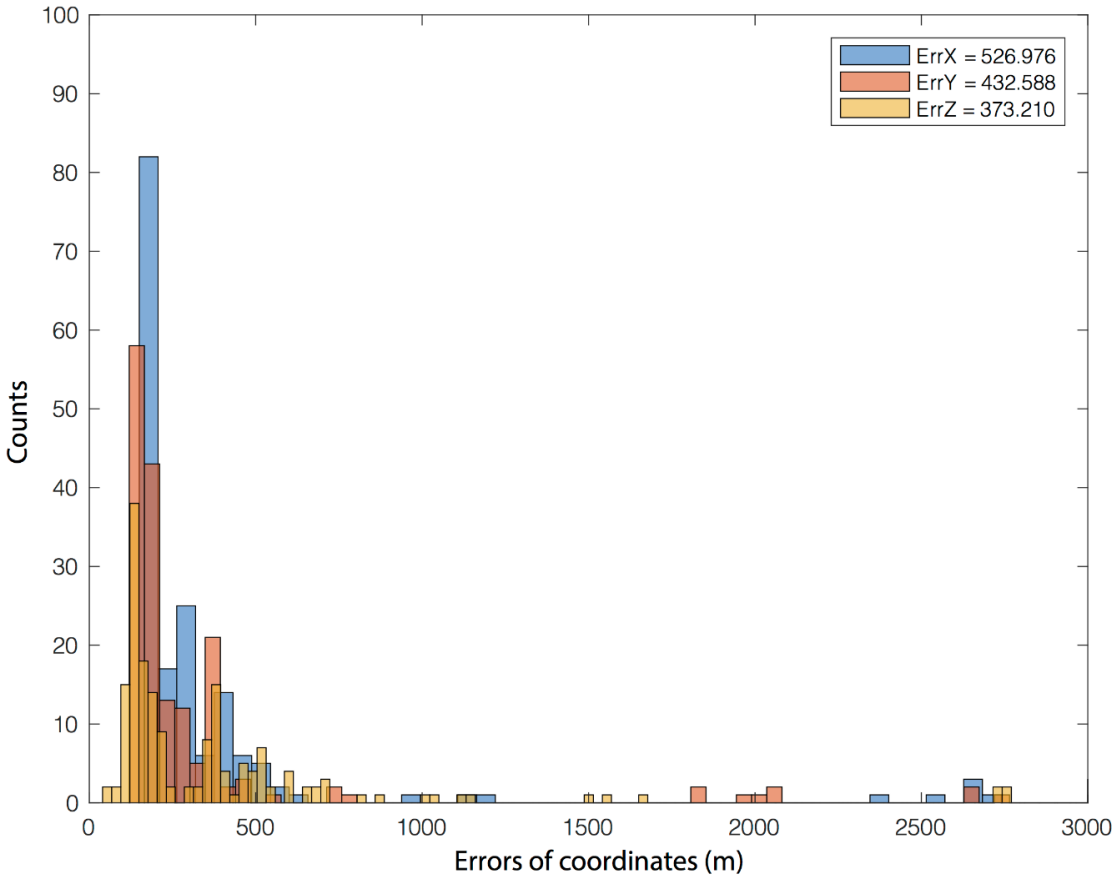

Figure S3

Histograms, representing seismic locations' errors on the three components x, y, and z, in blue, orange, and yellow respectively, computed by means of the SVD inversion on a subset of well-constrained events.

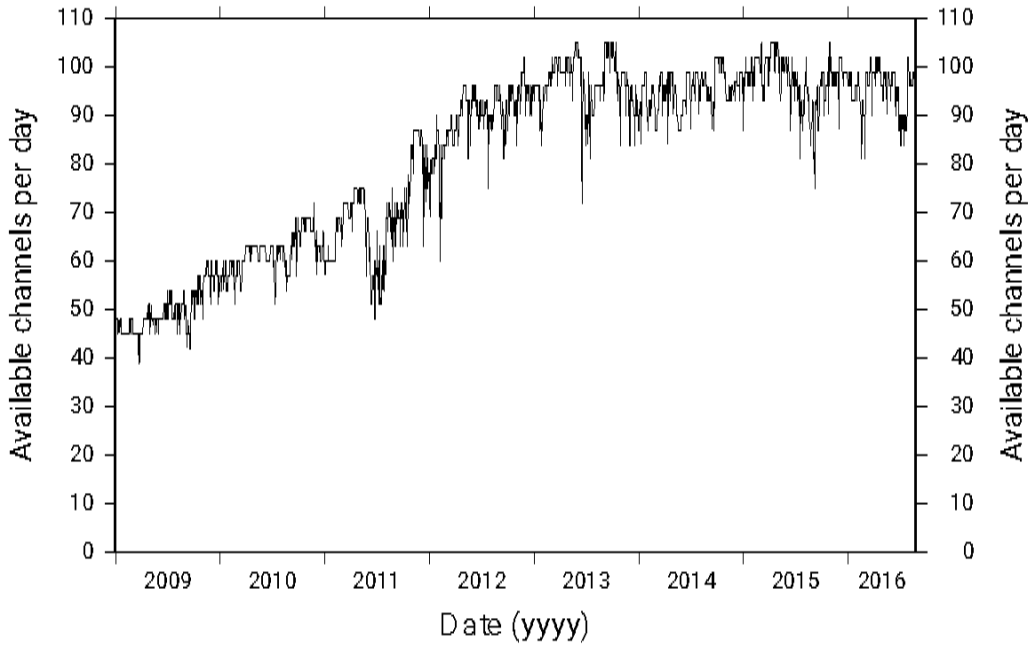

Figure S4

Seismic data channels available over time: the black line indicates the number of data channels available for template matching detection over time

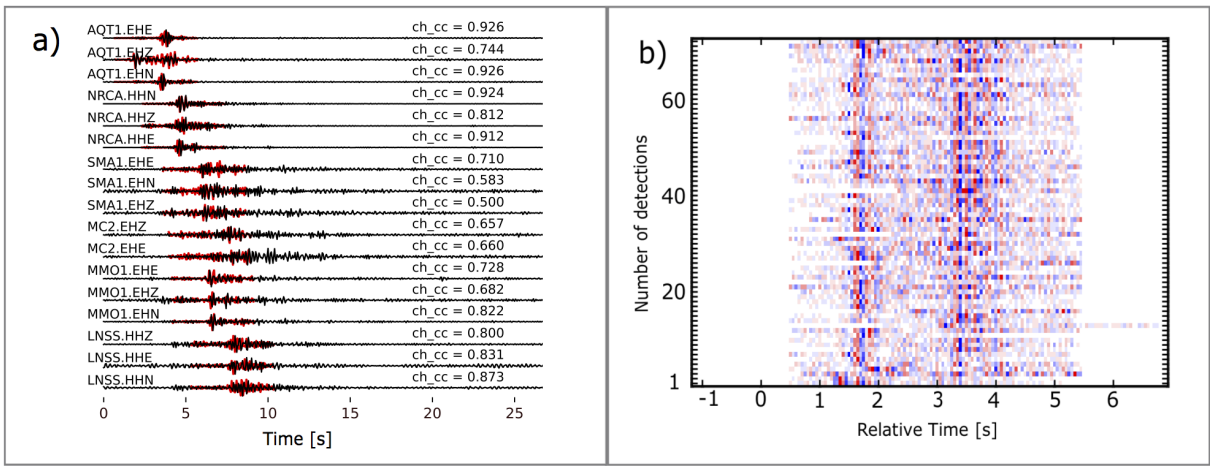

Figure S5

a) Example of a new detected event (origin time: 2013-01-06T20:02:21.33) associated with the template 11106 (origin time 2013-01-06T12:42:26.51). In black the continuous seismic waveform, in red the template (5 second long) used. The cross correlation value (ch_cc) of every single channel is shown. b) Detections associated with the template 11106 recorded at station AQT1 on vertical component.

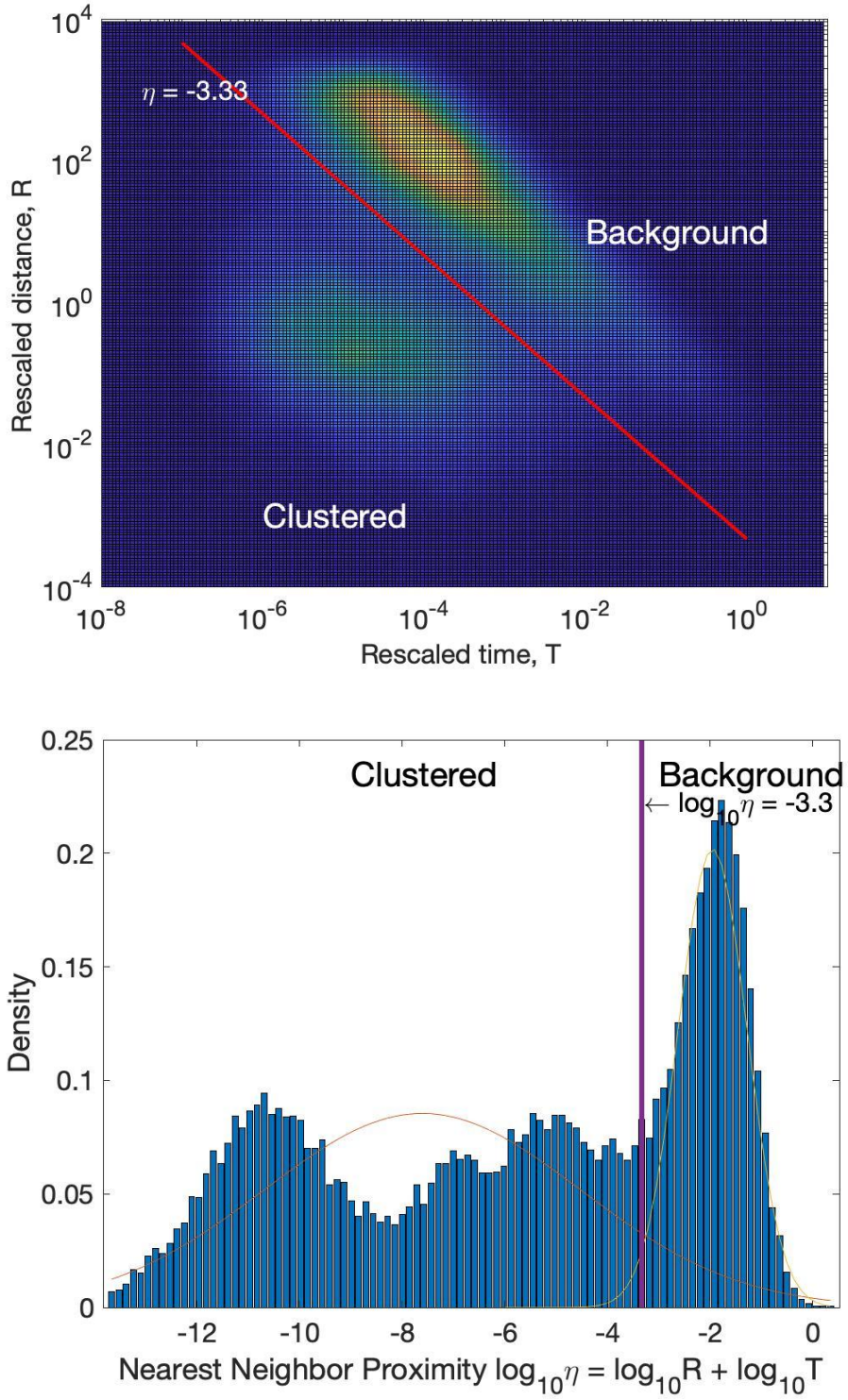

Figure S6

Top) Rescaled time and distance for clustered and background seismicity as obtained by applying a nearest neighbor proximity (Zalipin and Ben-Zion, 2016); bottom) Nearest neighbor proximity versus density for clustered and background seismicity as obtained by applying Zalipin and Ben-Zion, (2016).

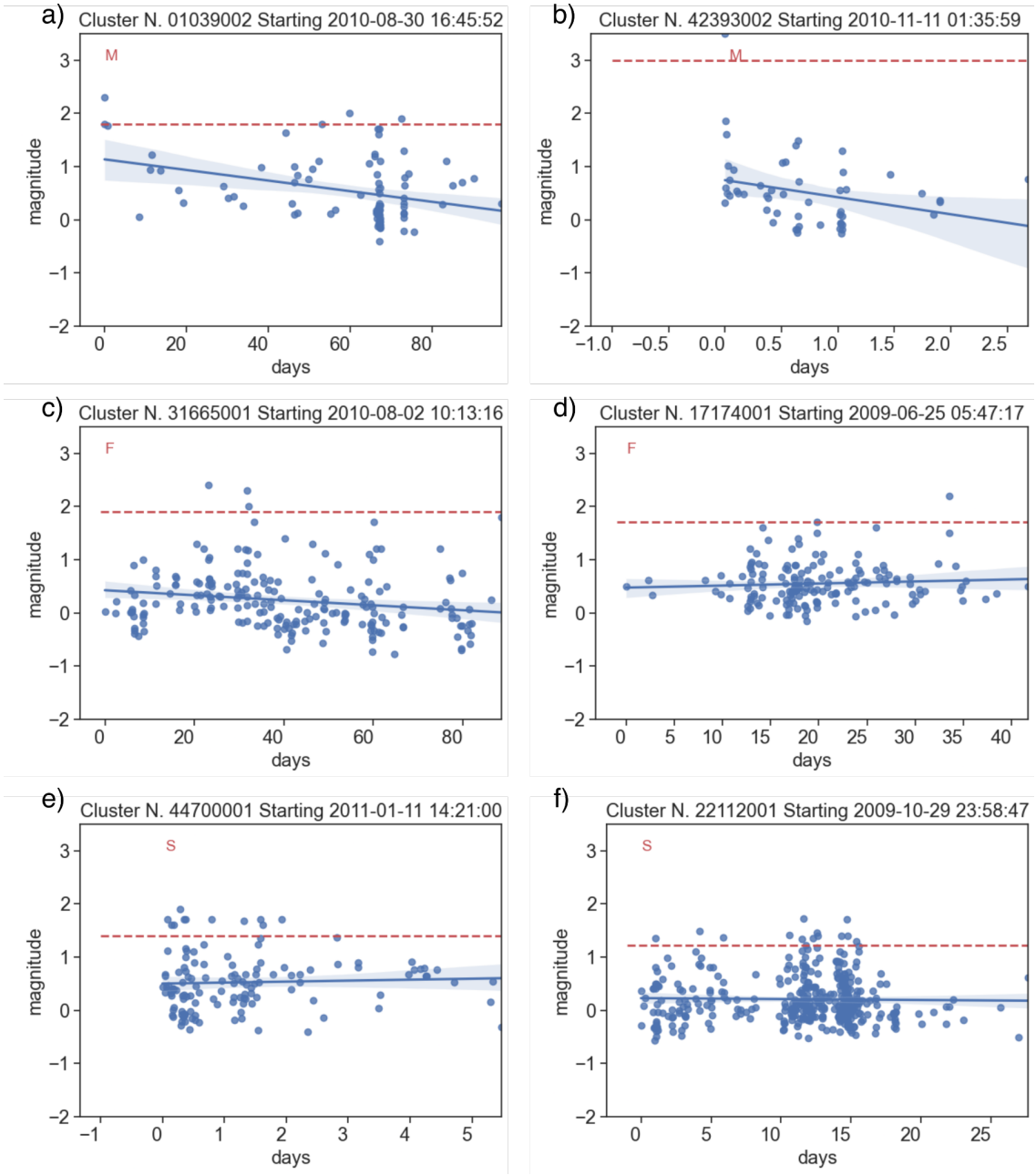

Figure S7

Duration and magnitude distribution of some clusters classified as a) and b) mainshock-aftershock sequences (M), c) and d) foreshock-mainshock (F), e) and f) swarm-like sequences (S). The red dotted line, defined as 0.5 magnitude degrees less than the maximum magnitude in a cluster, indicates the level to discriminate between swarms and foreshocks. If all the events preceding the maximum magnitude are below this threshold the sequence can be defined as a foreshock-mainshock. Swarms show many events above this level. The blue line represents a linear regression fit of the cloud of the events' magnitude and its uncertainty

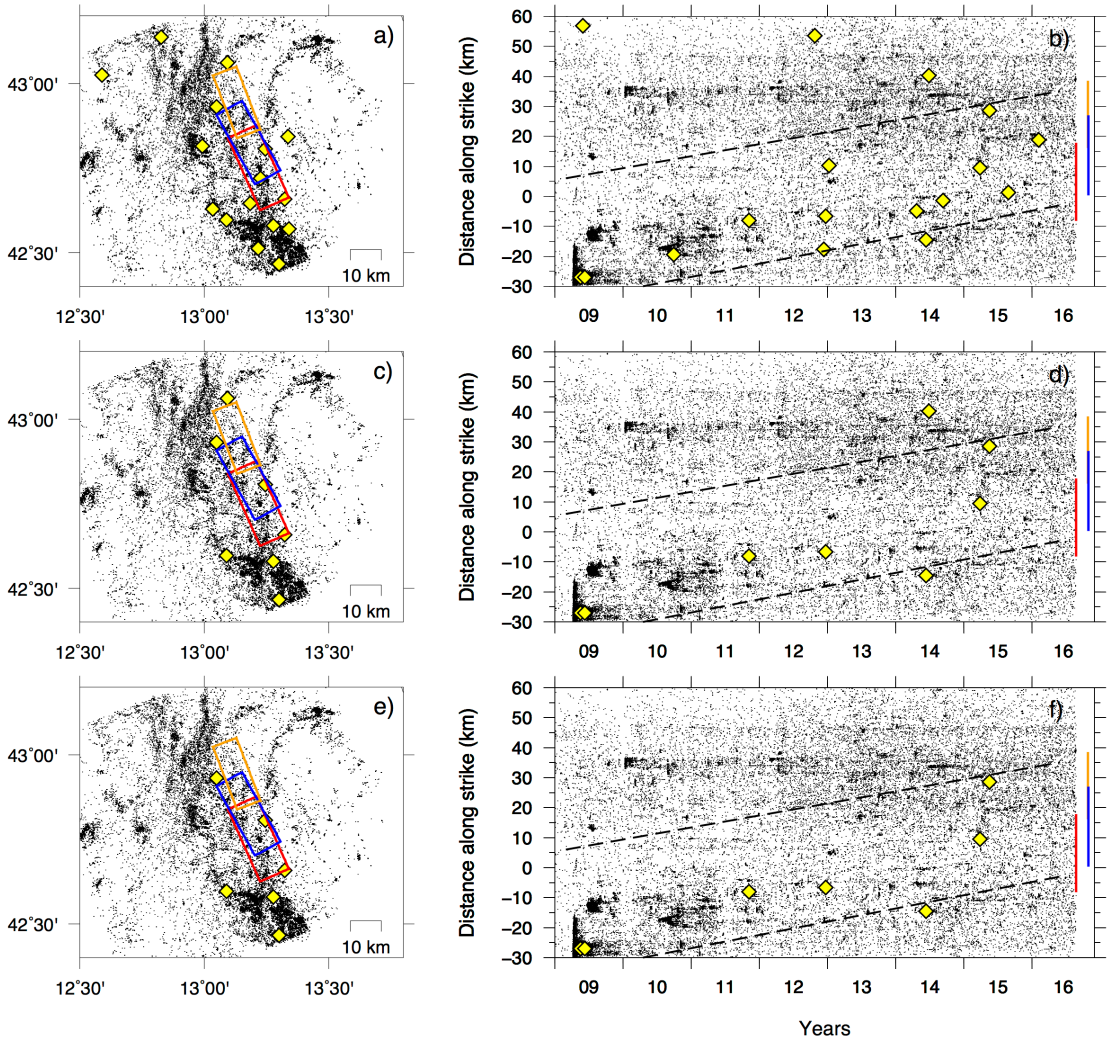

Figure S8

Location map (a) and time distance along strike section (b), showing the M>Mc seismicity (black dots) and the repeating earthquakes (yellow diamonds) found using configuration #1 in Table 1 (See Text S4 in the supplement). c) and d) the same, using configuration #2; e) and f) the same using configuration #3. In the along strike section, seismicity is projected along the 2016 main faults mean strike (336 degrees – N24W) with positive and negative offset values toward the north and south of the 24th of August Amatrice mainshock hypocenter (0 km distance). Faults are projected at the surface and along strike for the Amatrice mainshock (red), Visso (orange), and Norcia (blue). The dashed black lines mark the cluster migration shown in Figure 3c.

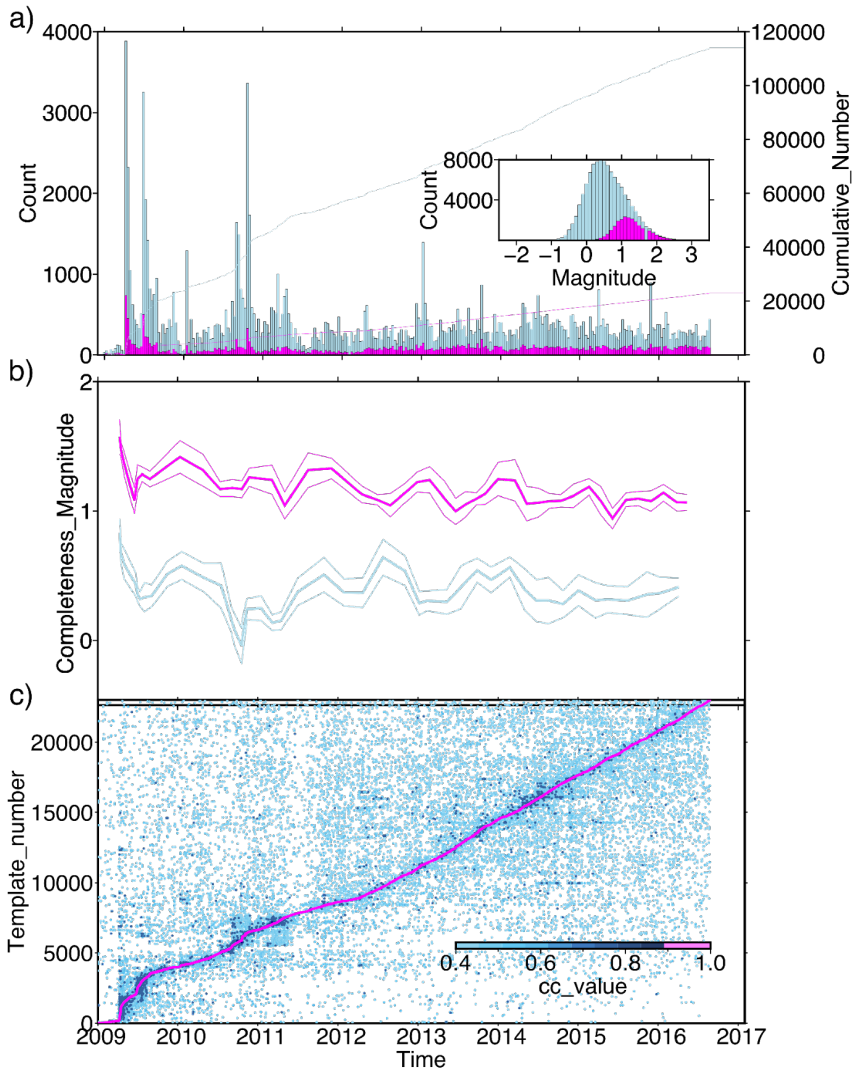

Figure S9

a) Templates (magenta) versus new detections (light blue) histograms from 2009 to 24th August 2016. In the inset of a), we also show the number of events versus magnitudes. b) Completeness magnitude (Mc) of templates (magenta) and the augmented catalog versus time (light blue). The Mc is calculated by averaging two methods, the maximum curvature method (Wiemer and Wyss, 2000) and the method based on b-value stability (Cao and Gao, 2002); solid thick lines mark the average value, thin lines +/- one standard deviation. We used time window of 250 events with 50% overlap. c) Time distribution of templates (magenta line) and associated new detections. New events are color scaled accordingly with the average cross-correlation value of detection. The diagram represents the ability of the templates to find new events before and after the template itself.

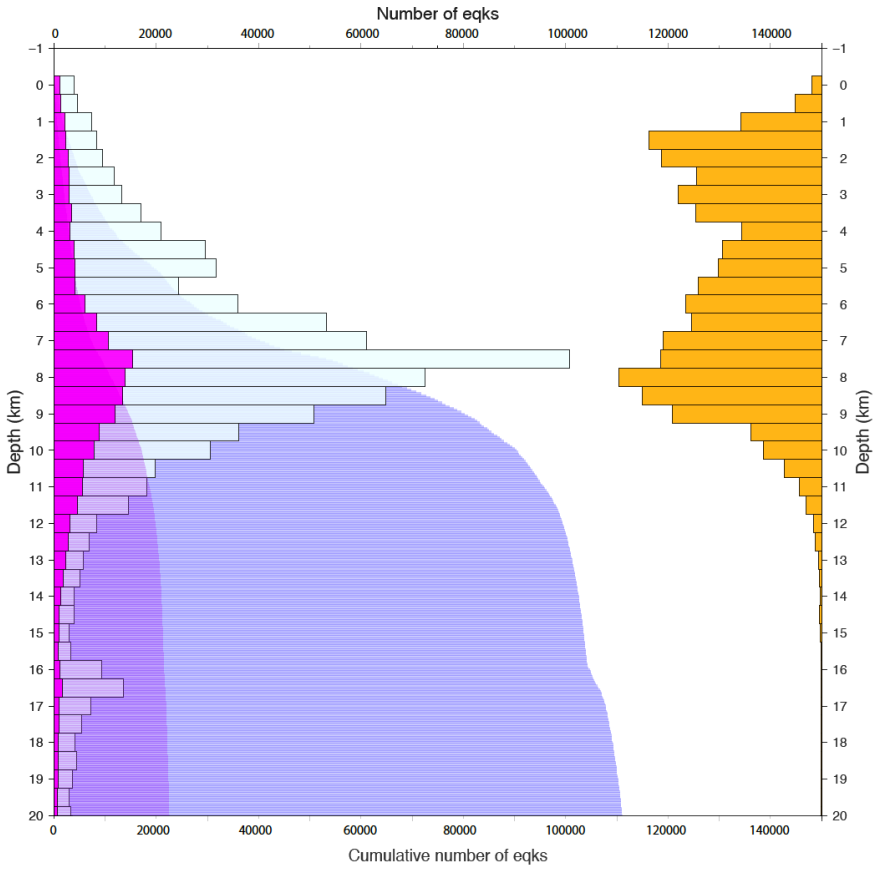

Figure S10

Histogram showing the depth distribution for templates in magenta (this study), augmented catalog in light blue (this study), and aftershocks in orange (Michele et al., 2020). Template and augmented catalog trends at depth are consistent, showing that seismicity concentrates in the 7-12 km range. Their cumulative number is also shown. Shallower seismicity is present with a lower number of events. Aftershocks activated a broad depth range.

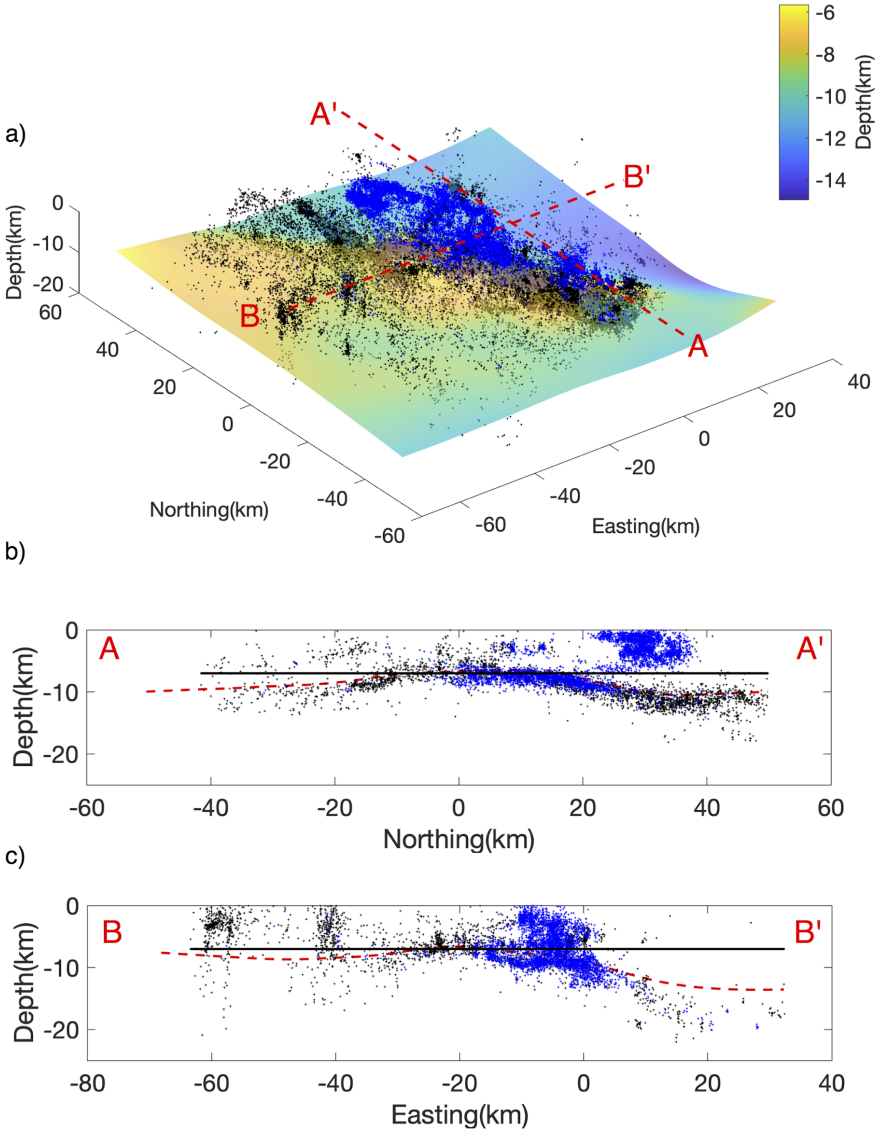

Figure S11

a) 3D surface of the Top of the Shear Zone (TSZ), dots correspond to templates (black) and aftershocks (blue); b) A-A' cross-section; c) B-B' cross-section. The red dashed line corresponds to the TSZ; the black horizontal line marks the 7 km depth as a reference. The sections cross the epicenter of 2016, 24th August mainshock. The definition of TSZ at variable depths is possible because of the presence of a thin layer (~ 1 km) showing less microseismicity (Vuan et al., 2017) and partially separating the shallow extensional fault system activated during the sequence from the underlying shear zone seismicity. The TSZ east-dipping boundary is more evident below and north of the 2016 fault system, identified by the aftershocks (in blue) located above 7 km depth.

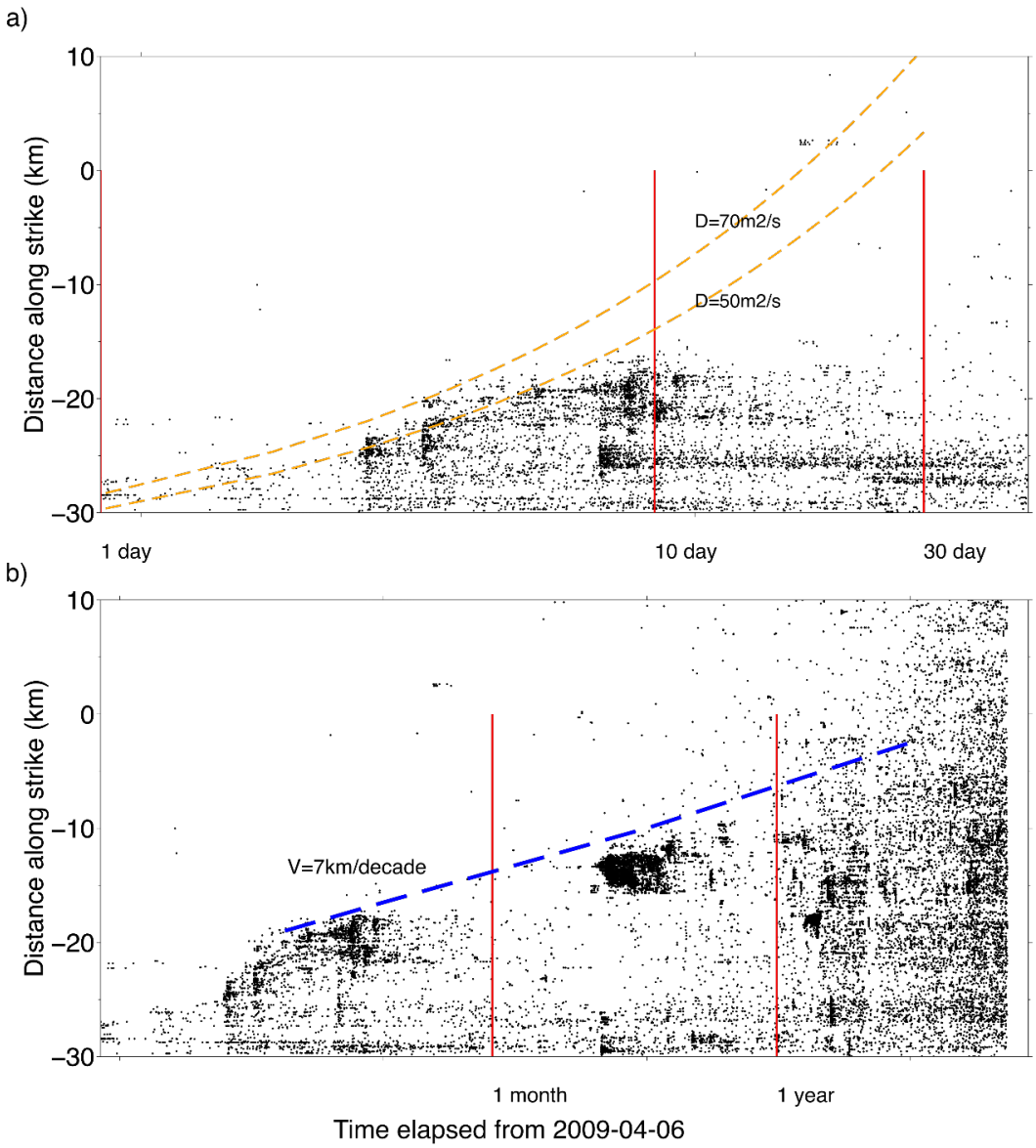

Figure S12

a) 30-day RT plot from 2009-04-06 of the augmented catalog. 50-70 m^2/s diffusivity curves in orange after the 2009 mainshock. b) 2-years RT plot from 2009-04-06 of the augmented catalog. 7km/decade migration in seismicity is represented as a dashed blue line (decade = exponential scale in days). Seismicity is projected along the 2016 main faults mean strike (336 degrees – N24W) with positive and negative offset values toward the north and south of the 24th of August Amatrice mainshock hypocenter (0 km distance). Only events with M>=Mc are plotted.

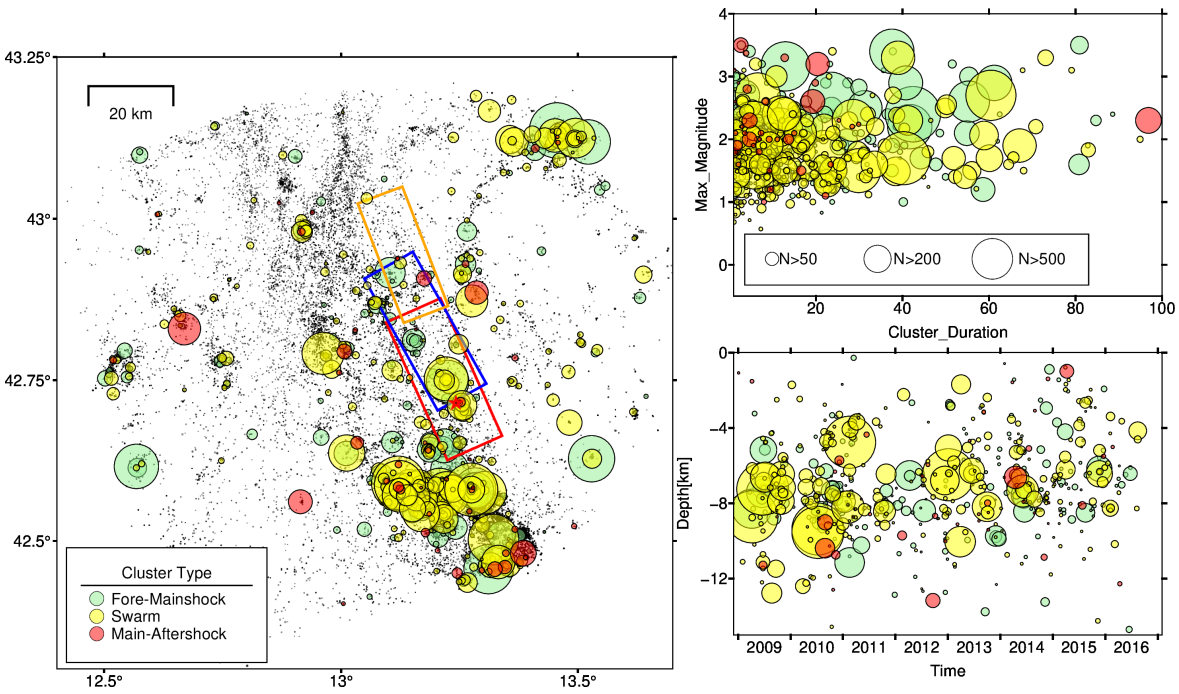

Figure S13

a) Layout map of different types of clusters. We represent clusters having a number of events greater than 10, b) maximum magnitude versus duration of the clusters of panel c), and depth versus time of the same dataset. Mainshock-aftershock sequences are under-represented in consideration of the small magnitudes involved and the 10 events cutoff used to select the clusters. Only events with M>=Mc are plotted.

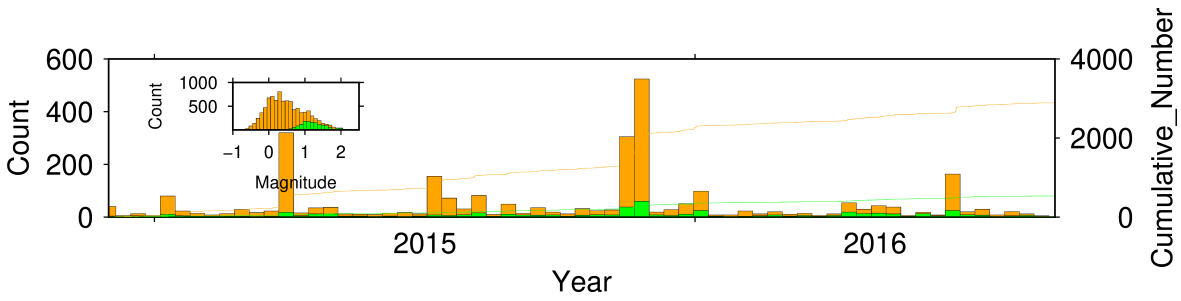

Figure S14

Number of events and cumulative number of events from 2015 to 24th August 2016 in the Amatrice fault volume (red box in Figure 1). Original (templates) and augmented catalogs are shown in green and orange respectively. We do not observe seismic acceleration in the two months before the mainshock. In the inset, we also show the number of events versus magnitudes.

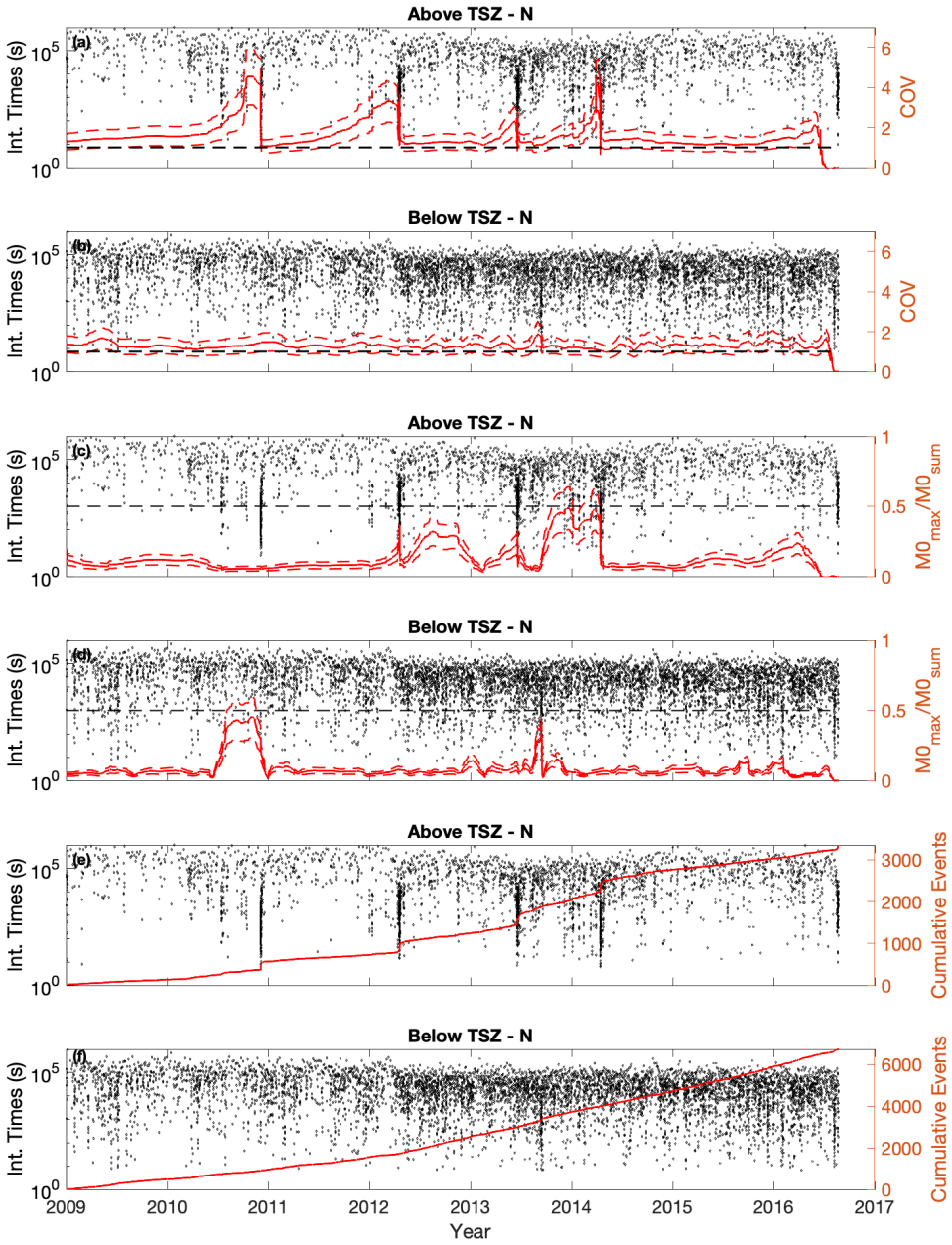

Figure S15

Coefficient of variation (COV) values of interevent times above (a) and below (b) the TSZ. Moment ratio (M0) of interevent times above (c) and below (d) the TSZ. Dashed lines show the associated standard deviation. The abrupt drop of coefficient of variation and moment ratio at the end of the analyzed time span in 2016 is related to the moving windows used, and should not be considered in the interpretation. The cumulative number of events above (e) and below (f) the TSZ. The analysis is performed for the northern volume (N in Figures 3a and b). Only events with M>=Mc are plotted.

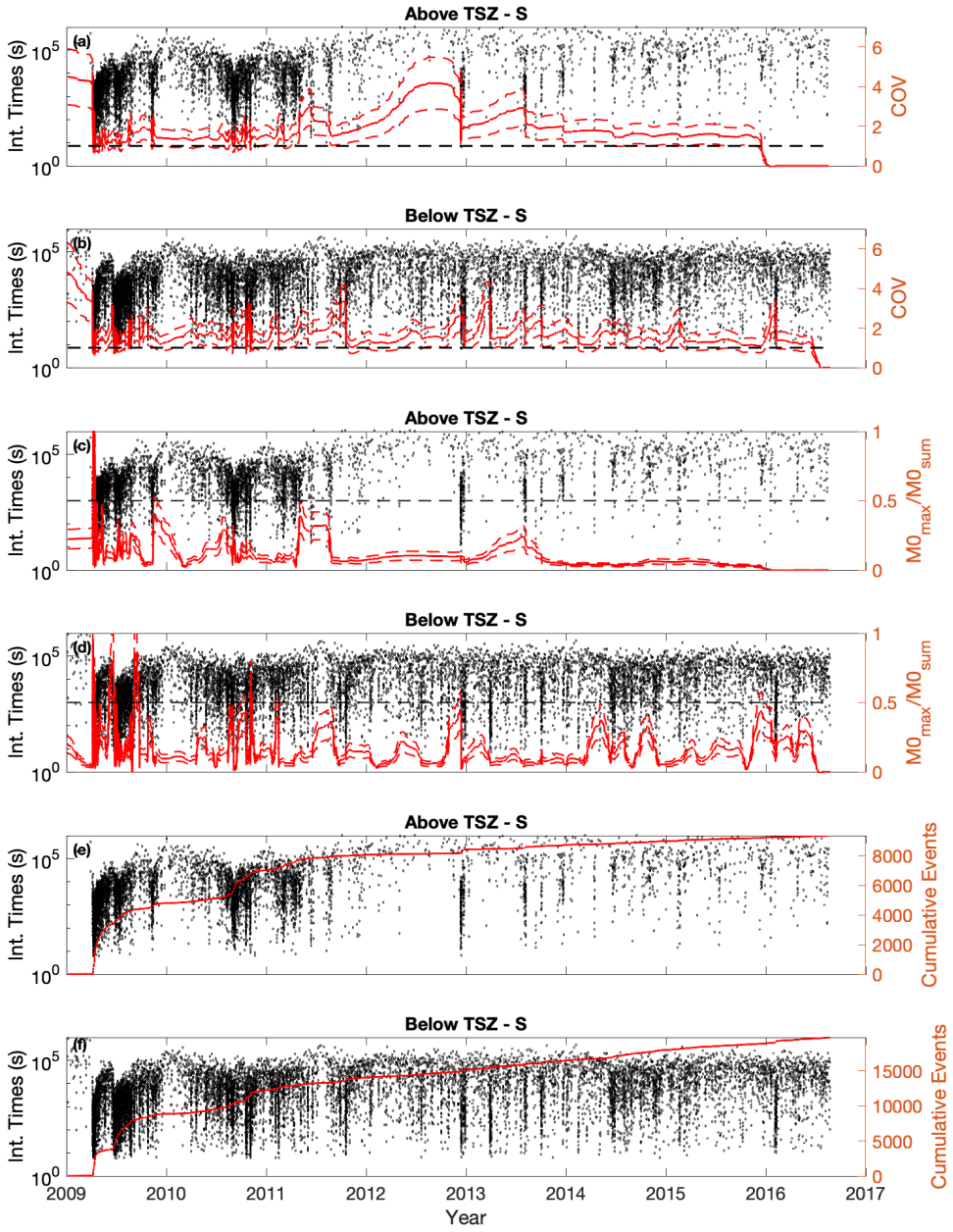

Figure S16

Coefficient of variation (COV) values of interevent times above (a) and below (b) the TSZ. Moment ratio (M0) of interevent times above (c) and below (d) the TSZ. Dashed lines show the associated standard deviation. The abrupt drop of coefficient of variation and moment ratio at the end of the analyzed time span in 2016 is related to the moving windows used, and should not be considered in the interpretation. The cumulative number of events above (e) and below (f) the TSZ. The analysis is performed for the southern volume (S in Figures 3a and b). Only events with M>=Mc are plotted.

STATION_LIST

Station	Latitude (deg)	Longitude (deg)	Elevation(m)
AQT1	42.7738	13.2935	770
AQU	42.3540	13.4050	710
ARRO	42.5792	12.7657	253
ASSB	43.0426	12.6587	734
ATCC	43.1851	12.6399	557
ATTE	43.1979	12.3536	929
CAMP	42.5358	13.4090	1283
CESI	43.0049	12.9046	840
CESX	42.6085	12.5868	380
CING	43.3756	13.1954	626
CSP1	43.0918	13.2048	1188
EL6	43.3293	13.1017	978
FAGN	42.2657	13.5838	761
FDMO	43.0365	13.0873	550
FEMA	42.9621	13.0498	1370
FIAM	42.2680	13.1172	1070
FOSV	43.2948	12.7612	559
GUMA	43.0627	13.3352	574
LNSS	42.6029	13.0403	1155
MC2	42.9114	13.1890	2
MDAR	43.1927	13.1427	940
MF5	42.9878	13.4597	723
MGAB	42.9126	12.1121	547
MMO1	42.8993	13.3268	957
MNTP	43.1374	13.4693	325
MOMA	42.8039	12.5701	1040
MURB	43.2630	12.5246	845
NRCA	42.8336	13.1143	927
OFFI	42.9350	13.6857	320
PF6	43.1379	13.1943	419
RM29	42.5606	13.2023	1276
RM32	42.5702	13.2932	1362
RM33	42.5090	13.2145	1097
SMA1	42.6305	13.3353	1150
SNTG	43.2550	12.9406	650
SRES	42.2370	12.5099	410
TERO	42.6228	13.6039	673

CATALOG_TM

Earthquake catalog obtained using the template matching technique from the 1st of January 2009 to the onset of the 2016 Central Italy sequence (24th of August 2016): it corresponds to a list of earthquake locations with magnitude estimation; the average cross correlation, the threshold, the associated template and the number of channels above the cross correlation threshold are indicated as well.

The catalog is available in Open Access Zenodo repository at: https://doi.org/10.5281/zenodo.7515062.